Inner-shell photoionization at relativistic energies

Dorin C. Ionescu,[1] Allan H. Sørensen,[1,2] and Ali Belkacem[1]
[1]*Lawrence Berkeley National Laboratory, University of California, 1 Cyclotron Road, Berkeley, California 94720*
[2]*Institute of Physics and Astronomy, University of Aarhus, DK-8000 Aarhus C, Denmark*
(Received 20 August 1998)

At relativistic energies the cross section for the atomic photoelectric effect drops off as does the cross section for liberating any bound electron through Compton scattering. However, when the photon energy exceeds twice the rest mass of the electron, ionization may proceed via electron-positron pair creation. The cross section for this channel saturates at several times the threshold energy, and hence the most probable way of photoionizing an atom at high energy is to make the vacuum spark. We present estimates for the cross section of this ''vacuum-assisted photoionization'' which proceeds either via direct pair creation on the bound electron or via pair creation on the atomic nucleus binding the inner-shell electron followed by an electron-electron or positron-electron encounter. [S1050-2947(99)05204-X]

PACS number(s): 32.80.Fb

I. INTRODUCTION

Inner-shell photoionization of an atom or an ion is one of the most basic processes in atomic collisions. With several very high-energy and high-intensity synchrotron x-ray sources existing or being built around the world, the physics of inner-shell photoionization has undergone a significant rebirth. Ionization may proceed through the photoelectric effect or Compton scattering. At MeV photon energies and beyond, the cross sections associated with both processes decrease with increasing photon energy $\hbar\omega$ essentially as $1/(\hbar\omega)$, making them very small in the highly relativistic energy regime [1–4].

In the relativistic regime an atom can be described as a many-body system containing Z electrons occupying discrete bound states, Z being the atomic charge number and, in the Dirac picture of hole theory, an infinite number of electrons occupying the negative-energy continuum. Atomic transitions with an energy scale of MeV and higher will bring into play the negative-energy continuum, allowing a new class of atomic collision processes to take place. For example, one such process is capture from electron-positron pair production in relativistic heavy ion collisions, a process that has been extensively studied over the last decade [5–9]. The interesting aspect of this process is that at relativistic energies a high-Z bare ion that impinges on an atom will preferentially pick up an electron from the vacuum instead of capturing an already existing bound electron of the target. This underlines the very important role that the QED vacuum plays in atomic collision processes at such high energies and in very strong fields.

The aim of this paper is to study photoionization at MeV energies and beyond, and to investigate the effects of correlations between the bound electron that is removed by this process and the Dirac sea. Indeed, when the photon energy exceeds twice the rest mass of the electron the negative-energy continuum will play an additional important role; photoionization of, say, the K shell can now proceed through a new channel in which the excess energy is taken by one of the negative-energy electrons. The final result is the creation of the K vacancy along with an electron-positron pair. Our present study shows that at highly relativistic energies the cross section of this new photoionization process becomes larger than the cross section of photoionization through Compton scattering or photoelectric effect. It is remarkable that we find here a feature similar to that in electron capture discussed above; that is, at high relativistic energies, photoionization of an atom or ion will proceed preferentially through ''sparking'' of the QED vacuum. We will call this new photoionization process *vacuum-assisted photoionization*.

The removal of the inner-shell electron through vacuum-assisted photoionization will result in the creation of two vacancies, one in the inner shell and the other in the negative-energy sea. This means that from a theoretical point of view this photoionization process can also be viewed as a double ionization by a single photon. Thus, one should expect many similarities in its theoretical treatment with the well-known photo double ionization of two bound electrons. An extensive literature discussing this latter process can be found. And because it is the simplest many-electron system, photo double ionization of helium has been the subject of a considerable number of theoretical and experimental studies over the last three decades [10–14]. Many tools that probe the electron-electron correlation for the various mechanisms that contribute to photo double ionization have been successfully developed, see McGuire *et al.* [10], and references therein.

Extending similarly detailed studies to vacuum-assisted photoionization will lead the research into the unique position of probing the fundamental dynamics and correlation of a bound electron and an electron from the negative-energy continuum. However, compared to photo double ionization, the situation is made somewhat more complicated by the presence of an extra lepton, the positron. The positron reflects the creation of a vacancy in the Dirac sea and this vacancy can interact after collision with the inner-shell electron. There is also an extra difficulty associated with the simplified description of the true QED vacuum in Dirac's hole theoretic picture since a rigorous theoretical treatment requires the solution of the relativistic many-particle problem in QED [15]. Finally, similar to the treatment of photo

double ionization of bound electrons, several different channels may contribute coherently, making a full treatment of the many-electron problem (using the quantum equations of motion and second quantization) quite difficult.

Our goal in this paper is to gain some insight into the physics that comes into play by limiting the scope of our work to very simple approximations that make the calculations tractable. We estimate the total cross section of vacuum-assisted photoionization and compare it to the cross sections of photoionization through Compton scattering and photoelectric effect. The photon energies of interest here are MeV and higher, that is, energies above the threshold for electron-positron production. Furthermore, since our goal is to study pair creation and ionization, we avoid complications associated with the initial interaction of bound electrons in atoms by considering a hydrogenlike ion.

We shall present different mechanisms by which vacuum-assisted photoionization can take place, but will examine in more detail only two fundamentally different mechanisms: In the first, the photon converts into an electron-positron pair in the field of the nucleus and, subsequently, the bound electron is ionized through an electron-electron or a positron-electron encounter. In the second mechanism, an electron-positron pair is produced in the field of the bound electron which in the process takes enough recoil to be freed from the atom or ion. The contributions of these two mechanisms to the total cross section are shown to be comparable in magnitude. However, the dependence of their respective cross sections on the atomic charge number of the target or on the quantum numbers of the initial inner shell is drastically different.

The paper is organized as follows. In Sec. II we briefly review photoionization through Compton scattering and the photoelectric effect. Section III is dedicated to calculations on and discussions of vacuum-assisted photoionization. In Sec. IV we present and discuss the results of these calculations and compare the cross sections of the various photoionization processes at relativistic energies.

II. PHOTOELECTRIC EFFECT AND COMPTON SCATTERING

In this section we shall give a brief discussion of the well-known inner-shell vacancy production mechanisms, photoelectric effect and Compton scattering. The discussion serves as a background for the discussion of vacuum-assisted photoionization in the following sections. We shall quote the basic cross-section formulas, which display the explicit dependence on target charge number Z and photon energy $\hbar\omega$. These formulas will be used in Sec. IV for comparison with the vacuum-assisted process. All cross sections to be listed are per electron rather than per atom.

Consider first the photoelectric effect. A useful formula for the cross section for K-vacancy production has been provided by Stobbe, cf. [16,17]. Stobbe applied the dipole approximation ignoring also retardation effects and performed a calculation based on exact nonrelativistic wave functions for a hydrogenlike ion. The cross section so obtained reads

$$\sigma_{\mathrm{Stobbe}}=2\sqrt{2}Z^5\alpha^4\sigma_T\left(\frac{mc^2}{\hbar\omega}\right)^{7/2}\times\left[2\pi\left(\frac{E_{1s}}{\hbar\omega}\right)^{1/2}\frac{\exp(-4\xi\cot^{-1}\xi)}{1-\exp(-2\pi\xi)}\right]. \tag{1}$$

Here $\alpha=e^2/\hbar c$ is the fine structure constant,

$$\sigma_T=\frac{8}{3}\pi r_0^2 \tag{2}$$

is the Thomson cross section, and $r_0=e^2/mc^2$ denotes the classical electron radius. The parameter ξ and the nonrelativistic binding energy E_{1s} are given as

$$\xi^2=\frac{E_{1s}}{\hbar\omega-E_{1s}},\quad E_{1s}=\frac{1}{2}(\alpha Z)^2mc^2. \tag{3}$$

It may be noted that the factor in front of the square brackets in Eq. (1) is the nonrelativistic perturbative result. At the absorption edge $\hbar\omega=E_{1s}$, the correction for nonperturbative effects, that is, the factor in square brackets in Eq. (1), assumes the value $2\pi\exp(-4)\simeq 0.12$.

An expression for K-vacancy production valid for low-Z materials when the photon energy is raised into the relativistic regime, $\hbar\omega\gtrsim mc^2$, has been obtained by Sauter by application of the Born approximation, cf. [16]. The expression, which is valid far from the absorption edge, reads

$$\sigma_K^{\mathrm{Born}}=\frac{3}{4}Z^5\alpha^4\sigma_T\left(\frac{mc^2}{\hbar\omega}\right)^5(\gamma_1^2-1)^{3/2}\left\{\frac{4}{3}+\frac{\gamma_1(\gamma_1-2)}{\gamma_1+1}\times\left[1-\frac{1}{2\gamma_1\sqrt{\gamma_1^2-1}}\ln\left(\frac{\gamma_1+\sqrt{\gamma_1^2-1}}{\gamma_1-\sqrt{\gamma_1^2-1}}\right)\right]\right\}. \tag{4}$$

The quantity $\gamma_1\equiv\hbar\omega/mc^2+1$ is the Lorentz factor for the emitted electron when binding effects are disregarded. It may be noted that for $\gamma_1\to 1$ Eq. (4) reduces to the nonrelativistic perturbation result, that is, to the front factor in Eq. (1). The high-energy limit of Eq. (4) is given by

$$\sigma_{\mathrm{Sauter}}=\frac{3}{4}Z^5\alpha^4\sigma_T\frac{1}{\gamma_0},\quad \gamma_0\equiv\frac{\hbar\omega}{mc^2} \tag{5}$$

and for brevity we shall call this the Sauter cross section. For corrections accounting for the nonperturbative nature of the interaction for high Z and $\hbar\omega\gtrsim mc^2$ we may refer to [17], see also [18,19]. The nonperturbative correction factor to multiply the Sauter cross section (5) in the high-energy limit assumes the values 0.97, 0.80, 0.52, 0.29, 0.22, and 0.20 for Z of 1, 8, 26, 55, 82, and 92, respectively, cf. [18].

Consider next Compton scattering. The cross section for scattering a photon of energy $\hbar\omega=\gamma_0mc^2$ on a free electron at rest is given as

$$\sigma_C=\frac{3}{4}\sigma_T\left(\frac{1+\gamma_0}{\gamma_0^3}\left[\frac{2\gamma_0(1+\gamma_0)}{1+2\gamma_0}-\ln(1+2\gamma_0)\right]+\frac{1}{2\gamma_0}\ln(1+2\gamma_0)-\frac{1+3\gamma_0}{(1+2\gamma_0)^2}\right), \tag{6}$$

cf. [16]. The nonrelativistic limit of the expression (6) is simply the Thomson cross section σ_T quoted in Eq. (2). At high energies the Compton cross section reads

$$\sigma_C=\frac{3}{8}\sigma_T\frac{1}{\gamma_0}\left(\ln(2\gamma_0)+\frac{1}{2}\right),\quad \hbar\omega\gg mc^2 \tag{7}$$

that is, a slightly slower falloff with increasing photon energy is encountered than for the photoelectric effect, compared to Eq. (5). Binding and motion of atomic electrons cause the cross section to drop below σ_T when the photon energy is decreased to the region of energies characterizing the atomic motion, see, for instance, Hubbell *et al.* [20], but such energies are not of concern here.

III. VACUUM-ASSISTED PHOTOIONIZATION

At sufficiently high photon energies ionization of an inner-shell electron may be catalyzed by the creation of an electron-positron pair. If E_B denotes the binding energy of the inner-shell electron, this process occurs with a threshold frequency $\omega_{\rm thr}$ of

$$\hbar\omega_{\rm thr}=2mc^2+E_B. \tag{8}$$

The inner-shell electron may be freed by electron-electron (positron-electron) interaction or by photon-electron interaction. In the first case we may think of pair creation in the field of the atomic nucleus followed by knock out of the inner-shell electron by one of the outgoing particles of the produced electron-positron pair. In the second case, we may think of, for instance, Compton scattering on the inner-shell electron (freeing it) followed by pair creation on the outgoing photon branch. The nucleus is not needed to propel this action. Or, still in the second case, we may think of pair creation directly on the inner-shell electron giving it a recoil sufficiently large that it leaves the scene. Also in this case, the presence of the nucleus is not required in order to mediate the transition.

A. Pair creation with $e^{\pm}$-e^- encounter

Consider electron-positron pair creation in the field of an atomic nucleus of charge Ze. The outgoing electron or positron collides with an inner-shell electron and transfers an energy to it which is larger than its binding energy E_B. Determination of the corresponding cross section according to the standard rules of quantum electrodynamics requires quite extensive calculations. We do not attempt such calculations here. Instead we shall make a simple semiclassical model which allows for estimates of cross sections.

In our model, the electron and the positron are created with equal probability anywhere inside a sphere of radius equal to the reduced Compton wavelength $\lambda\!\!\!^{-}_C=\hbar/(mc)$ $\simeq 386$ fm of the electron centered at the nucleus [21]. No correlation between the points where the electron and the positron first appear is assumed and also any interaction between the two is neglected. Hence the probabilities for knocking out a bound electron will be computed independently and added. From the point of first appearance each member of the pair is assumed to leave the scene on a straight path and we ignore the change in kinetic energy which classical mechanics would dictate due to motion in the background potential of the nucleus. For each of them, the probability for knocking out a bound electron is defined by the local electron density along the path (as defined by the quantum state of the target atom) and the cross section for transferring an energy larger than the binding energy E_B. Since relatively large energy transfers are of interest, we shall simply apply the cross section for collisions between free particles, that is, the Rutherford cross section (the finer details accounted for in the Møller and the Bhabha cross sections are neglected). The annihilation channel open to the positron when it encounters a target electron is discussed separately in Sec. III C.

With the above model it is obvious that the cross section for the process in question is related to the cross section $\sigma_{\rm PP}$ for pair production in the field of the nucleus by the simple relation

$$\sigma_1=\sigma_{\rm PP}\times P,\quad P=P_+ + P_-. \tag{9}$$

The quantities $P_\pm$ signify the knock-out probabilities for the electron and the positron. For the pair production cross section we may apply the Bethe-Heitler result, which pertains to the Born approximation, cf. [16]. It may be written as

$$\sigma_{\rm BH}=Z^2\alpha r_0^2\frac{28}{9}L. \tag{10}$$

The logarithmic factor L assumes at high energies the value

$$L_{\hbar\omega\gg mc^2}=\begin{cases}\ln(183Z^{-1/3})-1/42, & \text{Thomas-Fermi atom}\\ \ln(2\gamma_0)-109/42, & \text{bare nucleus,}\end{cases} \tag{11}$$

where, as noted, the upper expression is obtained for a nucleus whose field at large distances is screened out due to the presence of atomic electrons. Screening is important at very high energies; for lead, the two expressions in Eq. (11) are equal at $\gamma_0\equiv\hbar\omega/mc^2=275$, or 141 MeV. Near the threshold for pair production ($\hbar\omega=2mc^2$) the behavior of L is roughly $L\propto(1-2mc^2/\hbar\omega)^3$, cf. [22]. From threshold L increases smoothly over roughly two orders of magnitude in photon energy to the screened value in Eq. (11). The result for a bare nucleus listed in Eq. (11) applies approximately over most of the increase. Close to threshold the Born approximation actually fails, and production becomes somewhat more probable than this approximation predicts, at an energy of $3mc^2$ by a factor of 2 for a lead target, cf. [16]. At the same time the distribution over kinetic energy, which is identical for the electron and the positron in the Born approximation, becomes asymmetric due to attraction, respectively, repulsion by the nucleus.

The probability for knocking out the bound electron by, for instance, the positron is given within our model as

$$P_+=\left\langle\int_{E_B}^{E_+^{\rm kin}}dT\frac{d\sigma}{dT}\int_{z_0}^{\infty}dz n_B\right\rangle. \tag{12}$$

The average $\langle\ \rangle$ is an average over positron energies, point of creation, and emission direction ($E_+^{\rm kin}$ denotes the positron kinetic energy). The z axis is defined by the direction of the outgoing positron, z_0 denotes the z value of its first appearance, and n_B denotes the density of the bound target electron in its initial state. The differential cross section for transferring an energy T to the target electron is

$$\frac{d\sigma}{dT}=2\pi r_0^2\frac{1}{\beta_+^2}\frac{mc^2}{T^2}, \tag{13}$$

where the initial electron motion is neglected and the quantity β_+ represents the velocity of the positron in units of c.

The probability (12) factors as

$$P_+=\int_{E_B}^{\hbar\omega-2mc^2}dE_+^{\rm kin}f(E_+^{\rm kin})\int_{E_B}^{E_+^{\rm kin}}dT\frac{d\sigma}{dT}\left\langle\int_{z_0}^{\infty}dzn_B\right\rangle \equiv\Sigma_+\Phi_+, \tag{14}$$

where the average now is over point of creation and direction of exit only. We shall determine each of the two factors in Eq. (14) separately and start by considering the density factor Φ_+.

Let us assume the electron to be in the ground state of a hydrogenlike ion. Let a denote the nonrelativistic radius of the shell, $a\equiv a_0/Z$ with $a_0=\hbar^2/me^2=\alpha^{-1}\lambda\!\!\!^{-}_C$ being the Bohr radius of hydrogen (about 0.53 Å). In the extreme case $\lambda\!\!\!^{-}_C\ll a$, that is, at low atomic numbers Z, the creation point is essentially at the origin (on the scale of n_B). Hence

$$\left\langle\int_{z_0}^{\infty}dzn_B\right\rangle\rightarrow\int_0^{\infty}dzn_B,\quad \lambda\!\!\!^{-}_C\ll a \tag{15}$$

which is easily evaluated as

$$\int_0^{\infty}dzn_B=\frac{1}{4\pi}\left\langle\frac{1}{r^2}\right\rangle_{1s} =\frac{1}{2\pi a^2}\begin{cases}1, & \text{nonrelativistic}\\ [s(2s-1)]^{-1}, & \text{relativistic.}\end{cases} \tag{16}$$

The quantity s appearing in the relativistic result is defined as

$$s\equiv\sqrt{1-(\alpha Z)^2}. \tag{17}$$

It assumes the value 0.801 for lead. It may be noted that for lead, the relativistic result (16) is about twice the nonrelativistic value. However, for such a heavy target the approximation (15) does not apply—for lead $a=1.7\lambda\!\!\!^{-}_C$.

When we go beyond the region $\lambda\!\!\!^{-}_C\ll a$, that is, to moderate and high Z, two counteracting effects set in. One is that relativistic effects cause a higher degree of localization of the ground state so as to produce higher numbers; this is what Eq. (16) shows. The other is that with $\lambda\!\!\!^{-}_C$ no longer small compared to a, the average of the integral on the left-hand side in Eq. (15) will always be below that evaluated in Eq. (16). Using the symmetry of the ground state we may write

$$\left\langle\int_{z_0}^{\infty}dzn_B\right\rangle=\left(\frac{4}{3}\pi\lambda\!\!\!^{-3}_C\right)^{-1} \times\int_0^{\lambda\!\!\!^{-}_C}l(p)2\pi pdp\frac{1}{2}\int_{-\infty}^{\infty}n_{1s}(p,z)dz, \tag{18}$$

where $l(p)=2\sqrt{\lambda\!\!\!^{-2}_C-p^2}$. With a nonrelativistic hydrogenic ground state wave function, the last integral yields $(\pi a^2)^{-1}(2p/a)K_1(2p/a)$, where K_1 denotes a modified Bessel function. A similarly simple expression was not found in the relativistic case. Instead numerical calculation according to Eq. (18) shows that the result for the density factor when computed in units of $(\pi a^2)^{-1}$ varies only very little with the target atomic number. Within a few percent we have for all Z simply

$$\Phi_{\pm}=\frac{1}{2\pi a^2}. \tag{19}$$

As a consequence the density factor exhibits a Z^2 scaling.

Concerning the cross-section factor Σ_+ appearing in Eq. (14), let us first discuss the positron distribution $f(E_+^{\rm kin})$, associated with the pair creation in the nuclear field. First we note that well above threshold, this distribution is symmetric around the midpoint energy $\hbar\omega/2-mc^2$. However, close to the threshold energy, positrons tend to come out with higher energies than their negatively charged partners. At $\hbar\omega=3mc^2$, the positron kinetic energy is on average twice that of the electrons, cf. [16]. Despite such asymmetries which are intimately related to the aforementioned motion in the background potential of the nucleus, we shall assume $f(E_+^{\rm kin})$ to be symmetric in the following. Basically, we assume the production to be symmetric locally, and any asymmetries are considered to be due to the subsequent acceleration of the positron and deceleration of the electron as they (try to) leave the scene. Next we note that the distribution in question in general is rather flat. At extreme relativistic energies it has a broad minimum at the midpoint which is roughly two-thirds of the maximum obtained when one or the other of the charged particles takes all the energy available for distribution as kinetic energy. At moderate energies corresponding to, roughly, $20mc^2$ or lower, the distribution shows a broad maximum at the midpoint energy; the falloff towards zero at the two end points of the spectrum appears only within the last 10% or so of the energy range. Actually, very close to threshold, that is, for photon energies below roughly $3mc^2$, the distribution, as computed in the Born approximation where no asymmetry appears, varies essentially as $\sqrt{y(1-y)}$ where $y=E_+^{\rm kin}/(\hbar\omega-2mc^2)$, cf. [22]. In view of the generally flat distribution we shall simply make the substitution

$$f(E_+^{\rm kin})\rightarrow\frac{1}{\hbar\omega-2mc^2}. \tag{20}$$

By insertion of this expression and the Rutherford cross section (13) in Eq. (14) we end with the following estimate for the cross-section factor:

$$\Sigma_+\simeq\frac{2\pi r_0^2}{x_B}\left[1-\frac{x_B}{\gamma_2}+\frac{1}{\gamma_2}\left(\frac{1}{2}-\frac{3}{4}x_B\right)\ln\left(\frac{\gamma_2}{x_B}\right) -\frac{1}{\gamma_2}\left(\frac{1}{2}+\frac{1}{4}x_B\right)\ln\left(\frac{\gamma_2+2}{x_B+2}\right)+\frac{x_B}{2\gamma_2^2}-\frac{1}{2\gamma_2}\right], \tag{21}$$

where $x_B=E_B/mc^2$ and $\gamma_2=\hbar\omega/mc^2-2$. The factor in square brackets tends to 1 at high photon energies and vanishes at threshold, $\hbar\omega=\hbar\omega_{\rm tr}$. For photon impact on hydrogenic lead, the square-bracket factor assumes values of 0.78, 0.91, and 0.96 at photon energies of 1.5 MeV, 2.0 MeV, and

3.0 MeV. Hence except very close to threshold, which in this example appears at 1.12 MeV, the cross-section factor is well approximated by the front factor in Eq. (21).

Collecting the above information, and multiplying by a factor of 2 by the assumption of equal probabilities for knockout by the created electron and positron, we end up with the following estimate for the probability that enters in Eq. (9):

$$P \simeq 2\frac{(\alpha^2 Z)^2}{1-s} = 2\frac{(\alpha^2 Z)^2}{1-[1-(\alpha Z)^2]^{1/2}}, \quad \hbar\omega \gtrsim 2\hbar\omega_{\rm tr}. \tag{22}$$

For $\alpha Z \ll 1$, the probability is $4\alpha^2$ and it changes only slightly for heavier elements [$0.90\times 4\alpha^2$ for $Z=82$]. In other words, our estimate for P is essentially Z independent and well approximated as

$$P \simeq 2\times 10^{-4}, \quad \hbar\omega \gtrsim 2\hbar\omega_{\rm tr}. \tag{23}$$

Note that for energies below, roughly, twice the threshold energy the variation due to the square-bracket factor in Eq. (21) should be taken into account in the estimates (22) and (23). In this region asymmetries in the pair production spectrum are also significant.

With an essentially Z- and energy-independent probability, our estimate (9) for the cross section for pair creation with K-shell ionization, when the latter appears through electron-electron or positron-electron interaction, depends on atomic number and photon energy essentially as the Bethe-Heitler cross section for pair creation, Eq. (10). Hence we expect roughly a Z^2 scaling as well as a saturation of the cross section at high photon energies.

Estimates of the ionization of electrons bound in shells other than the K shell may be obtained in a similar manner. From the study of the density factor Φ_+ for the K shell as detailed in Eqs. (15)–(19) as well as by noting that the radii of higher shells are considerably larger than that of the K shell it is plausible to apply the approximation

$$\Phi_{\pm} \simeq \frac{1}{4\pi}\left\langle \frac{1}{r^2}\right\rangle_{nl}^{\rm nr} \simeq \frac{1}{2\pi a^2 n^3(2l+1)}, \tag{24}$$

where the superscript nr stands for nonrelativistic and n and l are the main and orbital angular quantum numbers. To obtain the last result, a hydrogenlike ion was again assumed. For the cross-section factor Σ_+ the expression (21) still applies. Consequently, the estimate corresponding to Eq. (23) reads

$$P_{nl} \simeq \frac{2\times 10^{-4}}{n(2l+1)}, \quad \hbar\omega \gtrsim 2\hbar\omega_{\rm tr}. \tag{25}$$

As before the estimate is per electron in the particular state. With Eq. (25) the total probability for any completely filled shell is

$$P_{\rm shell} \simeq 4\times 10^{-4}, \quad \hbar\omega \gtrsim 2\hbar\omega_{\rm tr}. \tag{26}$$

For the case of lead or gold the total probability for ionizing the atom following a pair creation event would hence end up near 1.8×10^{-3} in this simple model.

B. Pair creation in the field of a bound electron

Different from the mechanism discussed in the preceding section where one member of the electron-positron pair produced in the nuclear field collides with a bound electron, in the case of pair creation by a photon on an initially bound electron the presence of the nucleus is not required by kinematics. Due to change in mass of the particle producing the field the threshold energy for pair creation is different from that encountered in the preceding subsection. In particular, for a pair to be produced in a collision of a photon with an electron at rest the photon energy ω must exceed $4mc^2$, i.e., twice the threshold energy for pair creation in the nuclear field. In order to have a more compact notation we use in this subsection natural relativistic units ($\hbar=m=c=1$), unless otherwise stated. In these units length is measured in units of the reduced Compton wavelength $\lambda\!\!\!^{-}_C$ while momentum and energy are measured in units of mc and mc^2, respectively.

The differential cross section for pair production in the field of free unpolarized electrons was derived by Votruba [24] in lowest order perturbation theory. Compared with the Bethe-Heitler cross section for nuclear pair production by a photon given in Eq. (10), the calculations are considerably more complicated due to recoil and exchange effects. More precisely, retardation effects become important since the recoil velocity of the initial electron is not negligible in comparison with the speed of light. In addition, one has to take into account exchange terms which are associated with the indistinguishability of the two electrons and also radiative corrections.

In the lowest order of QED this process is described by elements of the third order scattering matrix $S_{\rm QED}^{(3)}$ connecting one photon state and three fermion states, i.e., two electrons and one positron, and one has to consider a total of eight Feynman diagrams when the four exchange diagrams are included. In the corresponding direct Feynman diagrams shown in Figs. 1(a)–1(d) the incoming photon and the initial electron have four-momenta k and p_i, and the outgoing leptons have momenta p_f, p_e, and p_p, respectively. While diagrams 1(a)–1(d) contribute also in the case of nuclear pair production, the additional four exchange diagrams (a_{ex})–(d_{ex}) are associated with the indistinguishability of the two electrons in the final state. These diagrams are obtained from the direct ones by interchanging the electron momenta p_f and p_e in the final states. Due to the considerable complexity of the expressions associated with these eight Feynman diagrams which require the evaluation of traces containing products of up to six Dirac matrices in $|S_{\rm QED}^{(3)}|^2$ the common practice was to use approximations, either by considering nonrelativistic or high-energy limits [24]. By nonrelativistic limit is meant the region of photon energies $\omega - 4m \ll m$. In addition, extensive numerical calculations were performed in [25] where the cross section for electron-positron pair production by unpolarized photons on free electrons was computed for a wide range of photon energies.

Only relatively recently was an exact expression for the cross section of triplet production, i.e., pair creation in the field of a free electron, obtained by integrating analytically the fully differential cross section over the angles of the outgoing electrons, without any approximations [26]. The resulting energy-differential cross section $d\sigma/dE_p$ with respect

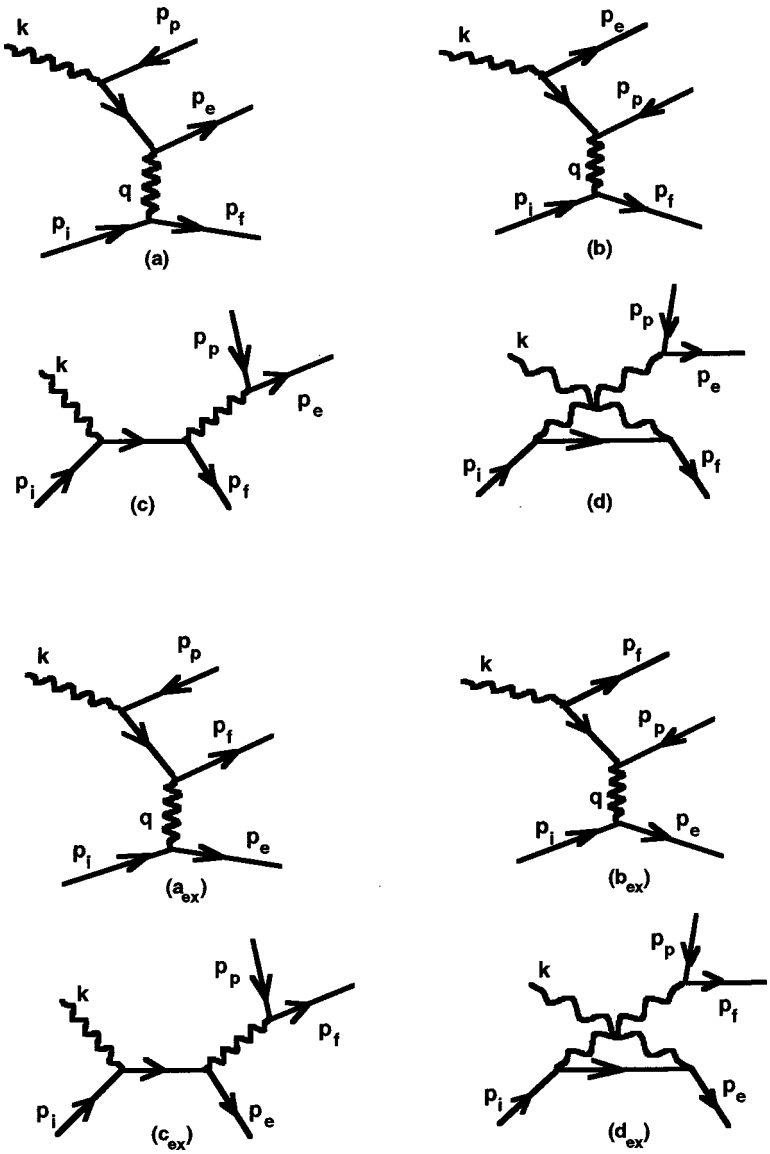

FIG. 1. Feynman diagrams for pair creation by a photon in the field of an electron. Diagrams (a) and (b) are referred to as Borsellino diagrams, and the Compton-like diagrams (c) and (d) are named γ-e diagrams. The corresponding exchange diagrams (a_{ex})–(d_{ex}) are obtained by interchanging the final electron lines, i.e., the four-momenta p_f and p_e of the electrons in the final states.

to the positron energy is thus evaluated by a one dimensional numerical integration over the angle ϑ_{kp} between the momenta $\vec{k}$ and $\vec{p}_p$ of the incoming photon and the produced positron, respectively. As a result of this important progress, the accuracy of the previous approximations as well as of the numerical cross-section calculations associated with this process could be rigorously determined.

In particular, it is seen that while the threshold approximation to the total cross section for triplet production [24]

$$\sigma_{\text{threshold}} = \alpha r_0^2 \frac{\pi\sqrt{3}}{4\times 3^5}(k-4)^2, \tag{27}$$

is valid only very close to $\omega = k = 4$, the results obtained in [25] by direct numerical integration are correct: For photon energies $4 \leqslant \omega \leqslant 16$ there is a good agreement with the results of Haug [26], the relative differences being less than 1.2%. In addition, the cross sections obtained in [26] cover the range of photon energies $4.001 \leqslant \omega \leqslant 5\times 10^3$, confirming Borsellino's results [27] for photon energies above 8 MeV. Borsellino [27] and Ghizzetti [28] have derived analytic expressions for the total cross section by neglecting the Feynman diagrams associated with the interaction of the initial electron with the photon, i.e., the so-called γ-e diagrams, as well as exchange effects: More precisely, they consider only diagrams (a) and (b) in Fig. 1. It is explicitly demonstrated in [25] that the neglected diagrams provide contributions with mutually opposite signs, such that they partially cancel out for $\omega \geqslant 15$. In addition, Borsellino derived a tractable although lengthy expression for the recoil momentum distribution $d\sigma_B/dq$, which turns out to be particularly useful for the present investigation.

Returning to the process in which an incoming photon creates a pair in the field of an initially bound electron one has to take into account also atomic binding effects. In other words, the outer and inner fermionic lines in Fig. 1 have to be associated with Coulomb-distorted wave functions and external-field Green's functions for electrons and positrons, respectively. However, the exact solution of such a treatment incorporating the electron-nucleus interaction exactly to all orders in αZ and the interaction with the incoming photon in third order is an extremely difficult task. Instead one may follow the approach of Maximon and Gimm [29] (see also [30]) in which atomic binding effects are accounted for ap-

proximately by considering inelastic scattering. In this specific approach the total cross section for pair creation in the field of a bound electron by a photon with momentum k is written as

$$\sigma(k)=\int_{q_m}^{q_0} dq I_{0n}(q)\frac{d\sigma_f}{dq}+\int_{q_0}^{q_M} dq\frac{d\sigma_f}{dq}, \tag{28}$$

where $d\sigma_f/dq$ is the recoil-momentum differential cross section, and $I_{0n}(q)$ is the incoherent scattering function associated with all possible excited states $n\neq 0$. For large momentum transfers, $q\geqslant q_0$, one has $I_{0n}(q)\rightarrow 1$ such that the electron is treated as free. For a discussion of the scattering function and related quantities see, for instance, [34,35]. The incorporation of binding effects through the scattering function $I_{0n}(q)$ is justified as long as the relevant momentum transfer q is small compared to momenta of the created fermions [30]. For the special case of a hydrogenlike ion in its ground state considered in the following one may use the relativistic expression for the incoherent scattering function

$$I_{0n}(q)=1-\left[\frac{\sin(2s\tan^{-1}Q)}{2sQ(Q^2+1)^s}\right]^2, \tag{29}$$

where $Q=q/(2\alpha Z)$ and the quantity s is defined in Eq. (17).

The integration limits q_m and q_M in Eq. (28) are the kinematic limits for the momentum transfer. For an initial electron at rest ($\vec{p}_i=\vec{0}$) one has

$$\vec{q}=\vec{p}_f=\vec{k}-\vec{p}_e-\vec{p}_p, \tag{30}$$

such that the allowed values for the recoil momentum $q_m \leqslant q\leqslant q_M$ are obtained in the laboratory system as

$$q_m=\frac{k(k-1)-(k+1)\sqrt{k(k-4)}}{2k+1}, \tag{31}$$

$$q_M=\frac{k(k-1)+(k+1)\sqrt{k(k-4)}}{2k+1}. \tag{32}$$

One may note that in the limit of very high photon energies the recoil momentum lies in the range $2/k\leqslant q\leqslant k$. In Eq. (28) q_0, which lies between q_m and q_M, is chosen so that $I_{0n}(q>q_0)\simeq 1$. Since the contributions associated with the six diagrams (c), (d), and (a_{ex})–(d_{ex}) in Fig. 1 are important for large momentum transfer, i.e., $q\gg 1$, only the second integral in Eq. (28) is relevant for these diagrams, see, for example, [29]. As a consequence, the first integral in Eq. (28) contains only the contribution of diagrams (a) and (b) of Fig. 1, enabling us to rewrite the total cross section as

$$\sigma(k)=\int_{q_m}^{q_M} dq\left\{\frac{d\sigma_B}{dq}+\left(\frac{d\sigma_f}{dq}-\frac{d\sigma_B}{dq}\right)-[1-I_{0n}(q)]\frac{d\sigma_B}{dq}\right\}$$
$$-\int_{q_m}^{q_0} dq\left(\frac{d\sigma_f}{dq}-\frac{d\sigma_B}{dq}\right)+\int_{q_0}^{q_M} dq[1-I_{0n}(q)]\frac{d\sigma_B}{dq}, \tag{33}$$

where we introduced the differential cross section $d\sigma_B/dq$ associated with Figs. 1(a) and 1(b) as derived by Borsellino [27]. While the last term in this expression vanishes by construction due to $I_{0n}(q)\simeq 1$ for $q\geqslant q_0$, the next to the last integral can be neglected since the cross sections σ_f and σ_B differ only in the contributions provided by the Compton-like and exchange terms, i.e., diagrams (c), (d), and (a_{ex})–(d_{ex}) in Fig. 1. As mentioned before, these contributions are negligible for small momentum transfers $q\leqslant q_0$. As a result, the final expression for the pair production cross section in the field of a bound electron may be written in the form given by Maximon and Gimm [29] as

$$\sigma(k)=\sigma_B(k)+\Delta\sigma_H(k)-\Delta S(k,Z). \tag{34}$$

The largest contribution in this expresson is provided by the first term

$$\sigma_B(k)=\int_{q_m}^{q_M} dq\frac{d\sigma_B}{dq}, \tag{35}$$

which represents the pair creation cross section in the field of a free electron by considering only the first two diagrams (a) and (b) in Fig. 1, i.e., the Borsellino diagrams. The second term in Eq. (34),

$$\Delta\sigma_H(k)=\int_{q_m}^{q_M} dq\left(\frac{d\sigma_f}{dq}-\frac{d\sigma_B}{dq}\right), \tag{36}$$

is associated with the remaining six diagrams of Fig. 1, i.e., the Compton-like and exchange diagrams. From Haug's work [26] one may see that for incident photon energies $\omega \geqslant 15$ the correction $\Delta\sigma_H(k)$ is always less than 1.2% of the total cross section $\sigma_f(k)$ in the field of a free electron. On the other hand, for photon energies $4<\omega<15$ the Compton-like and exchange contributions are important and $\sigma_B(k) > \sigma_f(k)$ so that the correction term $\Delta\sigma_H(k)$ is always negative in this energy range. The last term in Eq. (34),

$$\Delta S(k,Z)=\int_{q_m}^{q_M} dq[1-I_{0n}(q)]\frac{d\sigma_B}{dq}, \tag{37}$$

which is associated with screening effects, gives a nonvanishing contribution only for small momentum transfer, i.e., $q_m\leqslant q\leqslant q_0<1$. As we noted in the discussion following Eq. (28), for large momentum transfer the incoherent scattering function $I_{0n}(q)\rightarrow 1$, such that $[1-I_{0n}(q)]\rightarrow 0$, for $q\geqslant 1$. The quantity $Z\Delta S(k,Z)$ was calculated numerically and tabulated in [29] as a function of the photon energy for various elements up to lead.

In order to proceed further we consider in the following the total cross section $\sigma_B(k)$ for pair creation in the field of a free electron as derived in [27,28] by a direct evaluation of diagrams (a) and (b) in Fig. 1. In addition to an analytical expression of the total cross section in terms of an expansion in successive powers of $1/k$ through $1/k^7$ [28], in [27] an explicit representation of the differential cross section $d\sigma_B/dq$ is given in the form

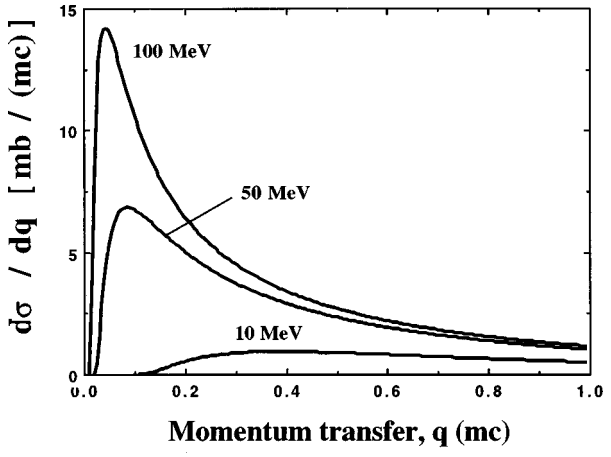

FIG. 2. Recoil-momentum differential cross section $d\sigma_B/dq$ for pair creation by a photon on a free electron as a function of the momentum transfer q for different values of the photon energy.

$$\frac{d\sigma_B(k,q)}{dq}=\frac{\alpha r_0^2}{k^2}\left[A(q,k)+B(q,k)\int_{q_m}^{q}dq'\,C(q',k)\right]\times\frac{q}{W(W-1)^2}. \tag{38}$$

Here, the quantity

$$W=\sqrt{q^2+1} \tag{39}$$

is the energy associated with the momentum transfer q. The different momentum-dependent contributions $A(q,k)$, $B(q,k)$, and $C(q,k)$ in Eq. (38) are explicitly given in [27], and will not be repeated here. In addition, in [29] the integral in Eq. (38) could be expressed in terms of dilogarithms, i.e.,

$$\int_{q_m}^{q}dq'\,C(q',k)=\frac{1}{2}\left\{\ln T\ln\frac{(T+W)^2-q^2}{T(W+q)}+L_2\left(-\frac{T}{W+q}\right)-L_2\left[\frac{-1}{T(W+q)}\right]\right\}, \tag{40}$$

such that the differential cross section (38) is further simplified. In the last expression the quantity T is defined as

$$T=k(q-W+1)-W+\sqrt{[k(q-W+1)-W]^2-1}, \tag{41}$$

and

$$L_2(x)=-\int_0^x dt\,\frac{\ln|1-t|}{t} \tag{42}$$

represents the dilogarithm function [31].

In Fig. 2 we show the differential cross section $d\sigma_B/dq$ for a free electron as a function of the momentum transfer q for different photon energies $\omega=10$, 50, and 100 MeV, respectively. It is seen that with increasing photon energies the recoil-momentum distributions attain their maxima at lower and lower values of the momentum transfer q. In addition, the maxima of the curves depicted in this figure become larger and larger in magnitude with increasing values of the photon energy.

The comparison of these momentum distributions with the corresponding exact distributions $d\sigma_{\rm Coul}/dq$ associated with pair production in a static Coulomb potential with $Z=1$ as derived by Jost, Luttinger, and Slotnik [33] provides further insight. In the work of Maximon and Gimm [29] it is shown that in the region of very small momentum transfer the differential cross sections $d\sigma_B/dq$ and $d\sigma_{\rm Coul}/dq$ approach the same distributions in the limit of high photon energies. On the other hand, for relatively high momentum transfers there are differences between these differential cross sections that are in general smaller than a factor of, roughly, 2 [29]. Suh and Bethe [32] showed that for very small momentum transfer, i.e., $q\ll 1$, the recoil energy taken by the particle producing the field is negligible compared to its rest mass, regardless of whether it is an electron or a nucleus. As a result, for photon energies of several hundred MeV and higher the recoil-momentum differential cross section $d\sigma_B/dq$ approaches the same limiting distribution as $d\sigma_{\rm Coul}/dq$, and the associated total cross sections σ_B and $\sigma_{\rm Coul}$ are essentially identical. However, with decreasing photon energy the differences between the two recoil-momentum differential cross sections become larger and larger such that for photon energies around 10 MeV the total cross section $\sigma_{\rm Coul}$ exceeds the cross section σ_B by a factor of 2 [29].

Having discussed the recoil-momentum differential cross section $d\sigma_B/dq$, we are now in a position to calculate the contribution of the mechanism of pair production in the field of the bound electron to the vacuum-assisted photoionization cross section. Since in the case of a bound electron momentum can be transferred both in excitation and ionization one has to exclude the channels in which the atom ends up in an excited state. This may be achieved in the simplest approximation by requiring that the allowed minimum momentum transfer q_m equals the momentum $q_{\rm cut}$ given by

$$q_{\rm cut}=\sqrt{(1+E_B)^2-1}, \tag{43}$$

which is needed to ionize the bound electron. Here, E_B represents the binding energy of the initial electron as given by the Sommerfeld formula for hydrogenlike ions, $E_B=1-\sqrt{1-(\alpha Z)^2}$ for the $1s$ state. Neglecting screening effects and the correction $\Delta\sigma_H(k)$ in Eq. (34), which are of minor importance in the energy range studied here, the total cross section $\sigma_2(k)$ for the vacuum-assisted photoionization process—regarded as pair creation in the field of a bound electron with the ionization of that electron—may be written as

$$\sigma_2(k)=\int_{q_{\rm cut}}^{q_M}dq\,\frac{d\sigma_B}{dq}, \tag{44}$$

with the maximum allowed momentum transfer q_M from Eq. (32).

C. Pair creation with subsequent annihilation

Positron annihilation is an additional source of vacancy production. Following the initial conversion of the incoming

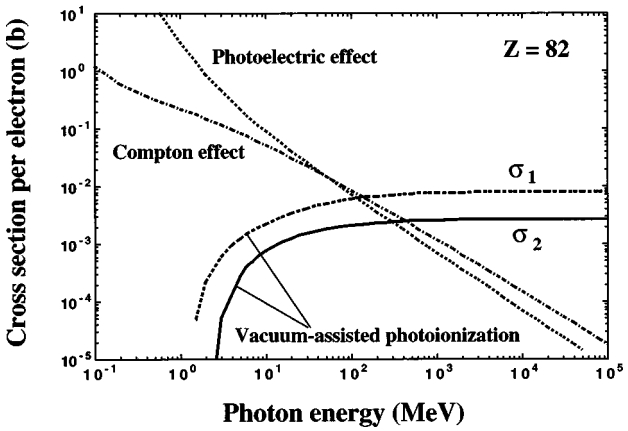

FIG. 3. Cross section for creation of a *K*-shell vacancy for lead ($Z=82$) for different photoionization processes as a function of the photon energy. The dashed-dotted line corresponds to the Compton effect and the dotted line to the photoelectric effect. Vacuum-assisted photoionization is represented by the dashed line (mechanism 1, i.e., pair production in the nuclear field with subsequent $e^{\pm}$-e^{-} encounter) and by the solid line (mechanism 2, i.e., pair production in the electron field), respectively. The cross sections are per *K*-shell electron.

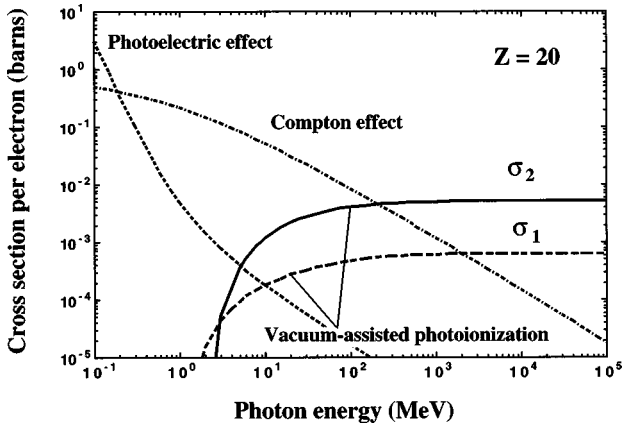

FIG. 4. Cross section for creation of a *K*-shell vacancy for calcium ($Z=20$) for different photoionization processes as a function of the photon energy. The dashed-dotted line corresponds to the Compton effect and the dotted line to the photoelectric effect. Vacuum-assisted photoionization is represented by the dashed line (mechanism 1, i.e., pair production in the nuclear field with subsequent $e^{\pm}$-e^{-} encounter) and by the solid line (mechanism 2, i.e., pair production in the electron field), respectively. The cross sections are per *K*-shell electron.

photon into an electron-positron pair, the positron may well subsequently annihilate on an inner-shell electron. The final product is an atom with an inner-shell vacancy, and an electron and two photons leaving the scene. In this subsection we shall estimate the strength of this channel through construction of a simple model along the lines of Sec. III A.

Let us assume the initial photoconversion to happen in the field of the atomic nucleus. All that is needed in order to estimate the relative strength of the annihilation channel is then an estimate of the probability $P_{\rm ann}$ that the positron, once created, will annihilate with an inner-shell electron. The ratio of $P_{\rm ann}$ to the probability computed in Sec. III A, cf. Eqs. (22), (23), and (25), will provide the estimate of the relative strength of the annihilation channel.

By the assumption of annihilation being a localized event requiring the annihilation partners to be at the same spot in space, the annihilation probability assumes a form similar to the knock-out probability given in Eq. (14), that is,

$$P_{\rm ann}=\int_0^{\hbar\omega-2mc^2} dE_+^{\rm kin} f(E_+^{\rm kin})\sigma_{\rm ann}(E_+^{\rm kin})\times\left\langle\int_{z_0}^{\infty} dz n_B\right\rangle \equiv \Sigma_{\rm ann}\times\Phi_+ . \tag{45}$$

The density factor is the same as before, cf. Eqs. (19) and (24). Determination of the requested ratio is hence reduced to determination of the ratio $\Sigma_{\rm ann}/2\Sigma_+$, where the factor of 2 in the denominator appears by the assumption of equal knock-out probabilities for electrons and positrons with equal velocities.

The cross section for (two-photon) annihilation of a non-relativistic positron on a free electron at rest reads

$$\sigma_{\rm ann}^{\rm rest}=\pi r_0^2/\beta_+ , \tag{46}$$

cf. [16]. As before, β_+ is the speed of the positron in units of *c*. Let us assume that the same expression holds for annihilation on an electron in bound motion only with replacement of the positron velocity by the relative positron-electron velocity. An upper limit of the cross-section factor $\Sigma_{\rm ann}$ for annihilation on a *K* electron is hence provided by replacing β_+^{-1} in Eq. (46) by $mc\langle p^{-1}\rangle_{1s}$. For the ground state of a nonrelativistic hydrogenlike ion this amounts to $16/(3\pi\alpha Z)$. Altogether we have

$$\Sigma_{\rm ann}\lesssim\frac{16r_0^2}{3\alpha Z}. \tag{47}$$

Comparison with Eq. (21) shows that, in general, the cross section σ_3 for vacuum-assisted *K*-shell vacancy production via annihilation is relatively small compared to σ_1, namely,

$$\frac{\sigma_3}{\sigma_1}\lesssim\frac{2}{3\pi}\alpha Z. \tag{48}$$

For a lead target, the right-hand side amounts to, roughly, 1/8. Close to threshold the square-bracket factor of Eq. (21) should be included but it does not significantly change the result. In conclusion, the magnitude of σ_3 is nowhere substantially larger than the uncertainty with which we have determined the cross section σ_1.

IV. RESULTS

In the preceding section we investigated the contributions to vacuum-assisted photoionization of inner-shell electrons by three different mechanisms that we assumed not to interfere with each other: pair production followed by electron-electron or electron-positron interaction (Sec. III A), pair production in the field of the bound electrons (Sec. III B), and pair production followed by the annihilation of the positron with the inner-shell electron (Sec. III C). The cross sections for the three mechanisms are referred to as σ_1,σ_2, and σ_3, respectively.

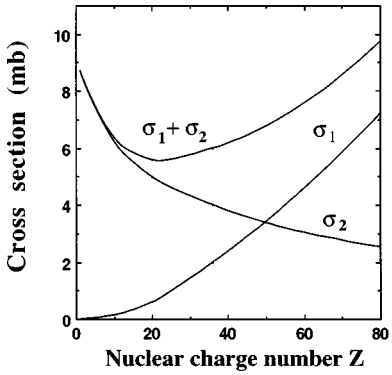

FIG. 5. Vacuum-assisted photoionization cross sections σ_1 and σ_2 associated with pair creation in the nuclear and electron field, respectively, as functions of the target atomic number Z. The upper curve corresponds to the sum $\sigma_1+\sigma_2$.

Figure 3 shows the cross section for creation of a K-shell vacancy in lead ($Z=82$) for the different photoionization processes discussed in the present paper except for the annihilation channel. In the preceding subsection it was shown that the contribution associated with positron annihilation is small, which is the reason the corresponding cross section is not displayed in this figure. The curves are drawn using tabulated values [20] for the photoelectric effect and Compton scattering, respectively, Eqs. (9), (19), and (21) for σ_1 with the product of the quantities on the right-hand side of the latter two making up half of the probability P appearing in Eq. (9) and with tabulated values [20] for the nuclear pair production cross section. For the cross section σ_2 associated with pair creation in the field of a bound electron we use Eqs. (43) and (44) as discussed in Sec. III B. Note that the cross sections are given per electron and one has to multiply by a factor of 2 to account for both K-shell electrons. From Fig. 3 one can see that the cross section for the creation of a K vacancy in Pb at photon impact energies below 1 MeV is dominated by the photoelectric effect. However, with increasing photon energy the photoelectric cross section decreases as a high negative power of the photon energy and then (above 10 MeV) as the inverse of the photon energy, see Eq. (5). The Compton cross section exhibits a slightly slower falloff, see Eq. (7). In contrast, the contribution from vacuum-assisted photoionization increases with increasing photon energy, starting from a threshold of approximately 1 MeV for σ_1 and 2 MeV for σ_2.

The contributions σ_1 and σ_2 saturate at 7.5 mb and 2.5 mb, respectively. The most important result displayed in Fig. 3 is that the total cross section of vacuum-assisted photoionization becomes comparable to the cross section of photoionization through Compton scattering and photoelectric effect for approximately 100 MeV photons and it dominates at higher energies. At 1 GeV, 90% of the cross section for creating a K vacancy is due to contributions from vacuum-assisted photoionization. This very interesting theoretical prediction can be tested experimentally with 1 GeV photons that are becoming available at several accelerator facilities, for example, through backscattering of laser photons on the 6 GeV electron beam at the European Synchrotron Radiation Facility (ESRF) in Grenoble, France. At even higher energies the removal of any atomic electron by photon impact will proceed almost exclusively through the vacuum-assisted process.

Pair production followed by electron-electron or electron-positron interaction provides the largest contribution to the cross section for the creation of a K-shell vacancy in Pb. This situation is reversed for Ca ($Z=20$) as shown in Fig. 4, where the largest contribution to the cross section comes from pair production in the field of a bound electron (σ_2).

This behavior is more clearly seen in Fig. 5 where the cross sections of the two mechanisms are shown as a function of the target atomic number Z. Pair production on a bound electron dominates for low-Z targets then decreases steadily as a consequence of the increased binding energy which requires higher and higher momentum transfer to free the electron. The contribution from the pair production in the nuclear field followed by electron-electron or positron-electron interaction increases almost as the square of the nuclear charge and subsequently dominates for high-Z atoms. Unlike the individual contributions, the sum of the cross sections of the two mechanisms changes by at most 30% over the whole range of atomic targets and exhibits a broad minimum around $Z=20$.

Finally, as we move to higher shells, the contributions to photoionization from the photoelectric effect, Compton scattering, and pair production are very different. The photoelectric effect brings almost no contribution to the creation of a vacancy in the higher shells while for Compton scattering the probability is proportional to the number of electrons in that shell. The contribution from vacuum-assisted photoionization is somewhat more complicated because of the very different behavior of mechanisms that contribute to the total cross section. As can be seen in Eq. (26), the probability to create a vacancy in any filled shell through the first mechanism (σ_1) is a number that approximately does not depend on the shell according to our simple model. The situation is again different for the second mechanism (σ_2) for which the probability to create a vacancy in any filled shell is proportional to the number of electrons in the shell multiplied by a factor between 1 and 4. This factor is higher for the higher shells. The multiplying factor is related to the binding energy of the shell that in turn dictates the minimum momentum transfer to free the bound electron, and hence its variation is similar to that of σ_2 in Fig. 5 which never exceeds a factor of, roughly, 3.

V. CONCLUDING REMARKS

In the present paper we make several approximations and build simple models to make the calculation of vacuum-assisted photoionization somewhat tractable. The price we pay, of course, is that our results should be considered more as a first estimate of the contribution of vacuum-assisted photoionization to the total photoionization cross section. The most important prediction of our calculations is that vacuum-assisted photoionization will dominate the other known photoionization processes at high energies. An interesting parallel can be made with capture from pair production which dominates charge transfer in relativistic heavy ion collisions. This highlights the crucial role that the negative-energy continuum plays in the relativistic regime in atomic collision processes. As we have seen, there are many physics

insights to be gained by our somewhat simple models. However, a close look at the extensive literature on photo double ionization will reveal several important limitations of the present calculations. For example, we used a semiclassical picture for the first vacuum-assisted mechanism (σ_1), and neglected the interference between the creation of the pair and the subsequent electron-electron or electron-positron interaction. This is obviously a gross approximation that is probably quite innacurate for high-Z atoms since the size of the K shell is comparable to the volume in which the pair is produced. As we pointed out in the Introduction, vacuum-assisted photoionization is in some sense similar to a photo double-ionization process. In particular, this means that the powerful theoretical tools developed in extensive studies of photo double ionization of atoms may be extended to develop a more rigorous relativistic description of vacuum-assisted photoionization.

ACKNOWLEDGMENTS

This work was supported by the Danish Natural Science Research Council, and by the Director, Office of Energy Research, Office of Basic Energy Sciences, Chemical Sciences Division, of the U.S. Department of Energy (DOE) under Contract No. DE-AC-03-76SF00098.

[1] J. C. Levin, G. B. Armen, and I. A. Sellin, Phys. Rev. Lett. **76**, 1220 (1996).

[2] L. Spielberger, O. Jagutzki, B. Krässig, U. Meyer, Kh. Khayyat, V. Mergel, Th. Tschentscher, Th. Buslaps, H. Bräuning, R. Dörner, T. Vogt, M. Achler, J. Ullrich, D. S. Gemmell, and H. Schmidt-Böcking, Phys. Rev. Lett. **76**, 4685 (1996).

[3] *X-ray and Inner-shell Processes*, edited by P. Lagarde, F. J. Wuilleumier, and J. P. Briand, special issue of J. Phys. (Paris) Colloq. **48**, C9-48 (1987).

[4] *Atomic, Molecular and Optical Physics Handbook*, edited by G. W Drake (AIP, Woodbury, NY, 1996); see section written by Bernd Crasemann, p. 701.

[5] A. J. Baltz, M. J. Rhoades-Brown, and J. Weneser, Phys. Rev. A **50**, 4842 (1994).

[6] A. Belkacem, H. Gould, B. Feinberg, R. Bossingham, and W. E. Meyerhof, Phys. Rev. A **56**, 2806 (1997).

[7] K. Rumrich, K. Momberger, G. Soff, W. Greiner, N. Grün, and W. Scheid, Phys. Rev. Lett. **66**, 2613 (1991).

[8] C. Bottcher, M. J. Rhoades-Brown, and M. R. Strayer, Phys. Rev. A **44**, 4769 (1991).

[9] D. C. Ionescu and J. Eichler, Phys. Rev. A **54**, 4960 (1996).

[10] J. H. McGuire *et al.*, J. Phys. B **28**, 913 (1995).

[11] R. Dörner, H. Bräuning, J. M. Feagin, V. Mergel, O. Jagutzki, L. Spielberger, T. Vogt, H. Khemliche, M. H. Prior, J. Ullrich, C. L. Cocke, and H. Schmidt-Böcking, Phys. Rev. A **57**, 1074 (1998).

[12] H. W. van der Hart, K. W. Meyer, and C. H. Greene, Phys. Rev. A **57**, 3641 (1998).

[13] P. J. Marchalant and K. Bartschat, Phys. Rev. A **56**, R1697 (1997).

[14] A. S. Kheifets and I. Bray, Phys. Rev. A **57**, 2590 (1997).

[15] W. Greiner, B. Müller, and J. Rafelski, *Quantum Electrodynamics of Strong Fields* (Springer-Verlag, Berlin, 1985).

[16] W. Heitler, *The Quantum Theory of Radiation* (Dover, New York, 1984).

[17] R. H. Pratt, Akiva Ron, and H. K. Tseng, Rev. Mod. Phys. **45**, 273 (1973).

[18] C. K. Agger and A. H. Sørensen, Phys. Rev. A **55**, 402 (1997).

[19] M. Gavrila, Phys. Rev. **113**, 514 (1959).

[20] J. H. Hubbell, H. A. Gimm, and I. Øverbø, J. Phys. Chem. Ref. Data **9**, 1023 (1980).

[21] This assumption may seem somewhat questionable, in particular, since, as is well known, screening plays an important role in moderating pair production at high energies, that is, in preventing an unlimited logarithmic growth of the cross section with increasing photon energy, cf. Eq. (11). The fact that screening is important at high photon energies means that distances of the order of the Thomas-Fermi screening length $\simeq \alpha^{-1} \lambda\!\!\!^{-}_C Z^{-1/3}$ are of importance at such energies. In an attempt to improve on the distribution in direct space, the distribution in recoil momentum could be inverted. We shall not embark on such a procedure. Instead we note that if we integrate the pair creation cross section (for screened nuclei) as given by Ter-Mikaelian [23] only over recoil momenta larger than $\alpha Z mc \simeq \hbar / a_K$, where a_K is the K-shell radius, then we obtain $0.50\sigma_{\rm BH}$ and $0.39\sigma_{\rm BH}$ at energies of $100mc^2$ and $1000mc^2$ for impact on a lead target. So even at such high energies and for such a heavy target we expect our estimate (19) for the density factor to be good within a factor of, roughly, 2.

[22] H. A. Bethe and J. Ashkin, in *Experimental Nuclear Physics*, edited by E. Segrè (Wiley, New York, 1953), Vol. I, p. 166.

[23] M. L. Ter-Mikaelian, *High-Energy Electromagnetic Processes in Condensed Media* (Wiley, New York, 1972). Cross-section differentials in recoil momentum may be found in Appendix I. Note, however, that many formulas, including the final (26), contain misprints.

[24] V. Votruba, Phys. Rev. **73**, 1468 (1948); Bull. Int., Acad. Tchèque Sci. **49**, 19 (1948).

[25] K. J. Mork, Phys. Rev. **160**, 1065 (1967).

[26] E. Haug, Z. Naturforsch. A **30A**, 1099 (1975).

[27] A. Borsellino, Rev. Univ. Nac. Tucuman Ser. A **6**, 7 (1947).

[28] A. G. Ghizzetti, Rev. Univ. Nac. Tucuman Ser. A **6**, 37 (1947).

[29] L. C. Maximon and H. A. Gimm, Phys. Rev. A **23**, 172 (1981).

[30] J. A. Wheeler and W. E. Lamb, Phys. Rev. **55**, 858 (1939); **101**, 1836(E) (1956).

[31] *Handbook of Mathematical Functions*, edited by M. Abramowitz and I. A. Stegun (Dover, New York, 1965).

[32] K. S. Suh and H. A. Bethe, Phys. Rev. **115**, 672 (1959).

[33] R. Jost, J. M. Luttinger, and M. Slotnick, Phys. Rev. **80**, 189 (1950).

[34] J. H. Hubbell, W. J. Veigele, E. A. Briggs, R. T. Brown, D. T. Cromer, and R. J. Howerton, J. Phys. Chem. Ref. Data **4**, 471 (1975).

[35] N. F. Mott and H. S. W. Massey, *The Theory of Atomic Collisions* (Clarendon Press, Oxford, 1949).